10TH INTERNATIONAL SYMPOSIUM ON PARTICLE IMAGE VELOCIMETRY
- PIV13
Delft, The Netherlands, July 1-3, 2013

Proper Orthogonal Decomposition based 3D microPIV: application to electrothermal flow study

Paul Kauffmann[1], **Sophie Loire**[1], **Igor Mezic**[1] **and Carl Meinhart**[1]

[1] Department of Mechanical Engineering, University of California, Santa Barbara, USA
kauffmann@engineering.ucsb.edu

ABSTRACT

Since late 1990's, micron-resolution particle image velocimetry (μPIV) has been widely developed to measure fluid flow velocities field in microchannels [1]. While 2D μPIV method has been extensively investigated, accurate 3D μPIV still remains challenging to implement since it usually requires specialized and expensive equipments (*e.g.* confocal, stereo imaging or holography microscopes) [2].

In the present work, the out-of-plane velocity component w is reconstructed from in-plane components (u,v), using fluid incompressibility. We use Proper Orthogonal Decomposition (POD) to decompose u and v into its dominant n eigenfunctions $\sum_{k=1}^{n} a_k(z)\phi_k(x,y)$ thereby filtering noise and simplifying the signal. In addition, those eigenfunctions are well suited to solve incompressibility equation since they enable independent differentiation and integration.

Our method is applied to an AC electrothermal fluid flow, which was previously studied experimentally and numerically[3].

1. Introduction

Micron resolution particle image velocimetry (μPIV) methods are being developed to visualize and quantify fluid flow velocities with a spatial resolution ranging from 0.1 to 100 μm. Two or more images are taken at a given time interval. The position of particles seeded in the liquid is then correlated thereby giving the displacement during that time interval and hence the flow velocity in a specific region of interest. The first successful μPIV experiment was conducted by Santiago *et al.* in 1998 [1], by adapting light sheet based macroscale PIV to measurement of microflows under microscope.

The technique is motivated by the advancements of microfluidics, which has been a growing field of physical science as well as an engineering technique for the past 20 years. Today, microfluidic devices are emerging on the market as new tools for many bio-engineering applications, such as bio-analytical assay, and pharmaceutical applications. The new phenomena inherent to microscale fluid flows and the precision needed for chemical and biological applications require robust measurement methods. For this reason μPIV has been widely used to study micro-flows [4, 2]. For instance, 2D μPIV has helped characterize electrokinetic phenomena [5, 6, 3], mixing [7], multiphase flows [8, 9], in vivo flows [10, 11] but also to analyse shearing flows applied on cells [12] or even to measure cell adhesion [13].

Yet, in many of these examples, fluid flows or forces on particles are three dimensional. For this reason, 3D μPIV is being developed to provide a full picture of the motion in microfluidics. In the wake of several 3D PIV techniques developed at macroscale, 3D μPIV techniques have been investigated. Digital Holography 3D μPIV [14, 15, 16] is based on the interference of one laser beam scattered from the object with its reference. The interference of the two beams on the recording plan gives 3D information on the object position, which is inaccessible to an object focused image. The main disadvantage of this technique is the particle density needs to remain low. Stereo Imaging [17] is an interesting alternative by using two cameras to obtain the out of plane information. However, accurate 3D imaging remains hard to obtain because of the conflict between spatial resolution and out of plane accuracy [2]. Such an experimental complexity can be reduced by using a defocusing technique. This technique uses a three pinhole aperture mounted on a single lens. The particle image through the three pinholes varies according to their position away from the focal plane [18], allowing a $5\mu m$ in plane and $1\mu m$ out of plane spatial resolution. To further decrease depth of field issues, which tends to limit out of plane resolution, confocal imaging based 3D μPIV was investigated in 2004 by Park *et al.* [19]. Since confocal imaging can record a single point at a time, this technique is not suitable for high velocity flows.

The 3D μPIV techniques presented above require special and expensive equipments and are not necessary easily implemented. The possibility of estimating the out of plane component of the velocity field using a standard epifluorescent microscope, was explored by Pommer *et al.* in 2007 [20] where the use of the incompressibility property of the fluid is proposed. Let

$\mathbf{u} = (u,v,w)^T$ be the local velocity vector with u, v and w, its components in the x, y and z direction, respectively. For steady or periodic fluid flows, the in-plane velocity, (u,v), is first measured on multiple 2D (x,y) planes by scanning a μPIV objective lens in the out-of-plane direction z. The out-of-plane component of velocity, w, can then be estimated by integrating the continuity equation for incompressible flow $\nabla\vec{u} = \partial u/\partial x + \partial v/\partial y + \partial w/\partial z = 0$, with respect to the z coordinate.

This technique is suitable for high particle density and high velocity flows. However, the derivation of measurement noise and uncertainties can easily dominate the calculated signal introducing large estimation errors. Moreover, the precision of the approximation of the integration is also highly dependent on the height at which velocity is computed [20].

To solve the issue of noise derivation and integration, we propose the use of Proper Orthogonal Decomposition (POD) [21]. POD has been used for image processing [22], signal analysis [23], and in fluid dynamics [24] ranging from oceanography [25] down to microfluidics [26]. The reason for such a broad application field is that this linear method permits to obtain low-dimensional approximate descriptions of a high-dimensional process and also reduce noise of data signals, by extracting the main eigenfunctions out of the signals. Using POD, a signal can be described by a finite sum in a variable separated form. The variable separation achieved by POD permits to solve the incompressibility equation by independent differentiation and integration of signal after POD. Using this property, POD has previously been used for macro PIV technique [27] but not yet for μPIV. The technique presented in this paper also proposes the use of a Savitzky Golay (SG) filter to analytically perform the necessary integration and differentiation. In 1964 Savitzky and Golay [28] provided a simplified method for calculating smoothing and differentiation of data by a least-squares polynomial fit technique. However in this approach, the traditional lengthy least-squares calculation is replaced by a simple, but equivalent, convolution. Since then, various modified (SG) filters have been proposed to improve smoothing and differentiation performance.

This paper describes how to use POD and a Savitzky Golay filter to extract the out of plane velocity component from planar components measured by μPIV at different heights with a classic epi-fluorescent microscope. This technique is applied to the full characterization of electrothermal vortices, which cannot be fully pictured with traditional 2D PIV techniques [3].

2. MicroPIV 3D velocity field evaluation

This section describes the Proper Orthogonal Decomposition (POD) and Savitzky-Golay filter based 3D velocity field evaluation by *μPIV* measurements of in plane velocities (u,v) on a collection of 2D (x,y) planes. Using this technique, the third component of the velocity field, w is extracted out of the 2D velocity fields.

Assuming the flow is incompressible, we can write:

$$\nabla.\mathbf{u} = 0 \tag{1}$$

Then,

$$\frac{\partial w}{\partial z} = -\left(\frac{\partial u}{\partial x} + \frac{\partial v}{\partial y}\right) \tag{2}$$

and the exact solution for out of plane velocity component, w is:

$$w(x,y,z) = -\int\left(\frac{\partial u}{\partial x} + \frac{\partial y}{\partial y}\right)dz + c(x,y,z_0). \tag{3}$$

where $c(x,y,z_0)$ is calculated assuming the velocity w is a priori known on the z_0 plane. This can be a wall boundary condition, $(w(x,y,z_0) = 0)$, or a plane of symmetry, $(\frac{\partial u}{\partial x}|_{z=z_0} = \frac{\partial y}{\partial y}|_{z=z_0} = 0)$.

2.1 Proper Orthogonal Decomposition (POD)

The proper orthogonal decomposition (POD) is a powerful and elegant method for data analysis aimed at obtaining low-dimensional approximate descriptions of a high-dimensional process. The POD provides a basis for the modal decomposition of an ensemble of functions, such as data obtained in the course of experiments.

The continuous velocities u and v can be written as:

$$u(x,y,z) = \sum_{k=1}^{n} a_{u,k}(z)\phi_{u,k}(x,y), \text{with} \int_x \phi_{u,i}\phi_{u,j} = \delta_{ij} \tag{4}$$

$$v(x,y,z) = \sum_{k=1}^{n} a_{v,k}(z)\phi_{v,k}(x,y), \text{with} \int_x \phi_{v,i}\phi_{v,j} = \delta_{ij} \tag{5}$$

with the expectation that with n tending to infinity, the approximation becomes exact, except possibly on a set of measured zero. From a mathematical point of view, $\phi(x,y)$ corresponds to the eigenfunction whereas $a(z)$ corresponds to the projection coefficient of the eigenfunction on to the function.

We use the Singular Value Decomposition POD method on the velocity components u and v, then equation 3 can be rewritten as:

$$w(x,y,z) = -\sum_{k=1}^{n_x n_y} \left[\frac{\partial \phi_{u_k}(x,y)}{\partial x} \int_{z_0}^{z} a_{u_k}(z)dz + \frac{\partial \phi_{v_k}(x,y)}{\partial y} \int_{z_0}^{z} a_{v_k}(z)dz \right] + c(x,y,z_0). \tag{6}$$

2.2 Savitzky-Golay Filter (SGF)

Experimentally, the coefficients $a_{u,k}(z_i)$, $\phi_{u,k}(x,y)_j$, $a_{v,k}(z_i)$ and $\phi_{v,k}(x,y)_j$ are discrete measurement values that contain noise, defined at every point of the experimental 3D grid. To perform the derivation and integration operations necessary to estimate the out of plane velocity component, w, we propose to utilize the polynomial fit given by a SGF, then analytically differentiate and integrate the polynomial.

Suppose $f(x)$ is the noise-free signal to be estimated and $f_\xi(x)$ the observed noisy signal due to an unknown noise $\xi(x)$:

$$f_\xi(x) = f(x) + \xi(x) \tag{7}$$

In experiments, the true signal $f(x)$ is measured with some errors and noise at discretely spaced spatial points x_i, $i = 1, \cdot, n_x$ and the resulting signal is a representation of $f_\xi(x_i)$.

The SGF can be applied to non-uniformly sampled data and even or odd number of filter points. Here, for simplicity, we will present only the case of uniformly sampled data x_i with spatial step size Δx, and a $(2M+1)$ point least squares polynomial fit across the data.

Let $s_k = k$ with $k = -M.\cdots, M$, $L^{n_p}(s_k) = [1, s_k, \cdots, s_k^{n_p}] \in \mathbb{R}^{n_p+1}$, $\theta = [a_0, a_1, \cdots, a_{n_p}] \in \mathbb{R}^{(n_p+1)\times(2M+1)}$, $F_\xi = [f_\xi(x_i + -M\Delta x), \cdots, f_\xi(x_i + M\Delta x)] \in \mathbb{R}^{2M+1}$, and $\Psi = [L^{n_p}(s_{-M}), \cdots, L^{n_p}(s_M)]^T \in \mathbb{R}^{(2M+1)\times(n_p+1)}$. Based on those notations, the SGF least square polynomial fit for grid point x_i is derived by solving the following optimization problem:

$$\min_\theta \sum_{k=-M}^{M} [f_\xi(x_i + k\Delta x) - \theta^T L^{n_p}(s_k)]^2 = \min_\theta |F_\xi - \Psi\theta|_2^2, \tag{8}$$

where $|\cdot|_2$ denotes the L_2 norm also called the Euclidean norm.

If $\Psi^T\Psi \in \mathbb{R}^{(n_p+1)\times(n_p+1)}$ is non-singular, then the optimal solution of 8 can be obtained explicitly as follows:

$$\tilde{\theta} = (\Psi^T\Psi)^{-1}\Psi^T F_\xi. \tag{9}$$

Let

$$h(s) = (\Psi^T\Psi)^{-1}\Psi^T L^{n_p}(s),\ \forall s \in \mathbb{R}, \tag{10}$$

then the SGF approximation of $f_\xi(x)$ centred at point x_i, is given by

$$\tilde{f}(x_i + s\Delta x) = \tilde{h}(s)F_\xi. \tag{11}$$

Note that $\tilde{h}(s)$ is completely defined by the choice of polynomial order n_p and filter width M and is independent of the data and data spatial step size.

Then, the derivative of $f_\xi(x)$, $\frac{\partial f_\xi(x)}{\partial x}$, SGF approximation centred at point x_i, is derived as:

$$\tilde{g}(x_i + s\Delta x) = \Delta x \frac{\partial \tilde{f}_\xi(x_i + s\Delta x)}{\partial s} = \frac{1}{\Delta x}\frac{\partial \tilde{h}(s)}{\partial s}F_\xi. \tag{12}$$

Let's define M_0 such that $x_0 = x_i - M_0\Delta x$. Similarly, the integral of $f_\xi(x)$, $\int_{x_0}^{x} f_\xi(z)dz$, SGF approximation centred at point x_i, is derived as:

$$\tilde{l}(x_i) = \Delta x \int \tilde{f}_\xi(x_i + s\Delta x)ds + C = \Delta x \int \tilde{h}(s)ds F_\xi + C. \tag{13}$$

2.3 Application of SGF and POD to the approximation of out of plane velocity component

The coefficients $a_{u,k}(z_i)$, $\phi_{u,k}(x,y)_j$, $a_{v,k}(z_i)$ and $\phi_{v,k}(x,y)_j$ are obtained from a SVD POD using equation (6). Modes are ordered by decreasing energy (decreasing singular values). The number of modes to be used n_{POD_x}, n_{POD_y} is then chosen.

The SGF matrix filter function $\tilde{h}(s)$ is derived for the experimental 3D grid for direction x, y and z separately ($\tilde{h}_x(s)$, $\tilde{h}_y(s)$, $\tilde{h}_z(s)$) using (10), where spatial steps are taken from the experimental 3D grid (Δx, Δy, Δz), the number of filter points M and polynomial order n_p are chosen. Note that M and n_p can be different for each direction.

From the coefficients $a_{u,k}(z_i)$, $\phi_{u,k}(x,y)_j$, $a_{v,k}(z_i)$ and $\phi_{v,k}(x,y)_j$ a matrix corresponding to the F_ξ matrix definition is extracted. They will be referred in the following as matrix $A_{u_k}(z)$, $\Phi_{u_k}(x,y)$, $A_{v_k}(z)$, $\Phi_{v_k}(x,y)$

Finally the approximation $\tilde{w}$ of the out of plane velocity component w can be estimated on the experimental 3D grid using the formula :

$$\tilde{w}(x,y,z) = -\frac{\delta z}{\delta x}\sum_{k=1}^{n_{POD_x}}\left[\frac{\partial \tilde{h}_x(s,y)}{\partial s}\Phi_{u_k}(x,y)\int \tilde{h}_z(s)dsA_{u_k}(z)\right] \quad (14)$$

$$-\frac{\delta z}{\delta y}\sum_{k=1}^{n_{POD_y}}\left[\frac{\partial \tilde{h}_y(x,s)}{\partial s}\Phi_{v_k}(x,y)\int \tilde{h}_z(s)dsA_{v_k}(z)\right] \quad (15)$$

$$+c(x,y,z_0). \quad (16)$$

where $c(x,y,z_0)$ is calculated assuming the velocity w is a priori known on the z_0 plane. This can be a wall boundary condition, $(w(x,y,z_0)=0)$, or a plane of symmetry, $(\frac{\partial u}{\partial x}|_{z=z_0} = \frac{\partial y}{\partial y}|_{z=z_0} = 0)$.

3. Material and Method

3.1 Experimental setup

The experiments are carried out on an AC electrothermal fluid flow setup previously studied through theory, models and experiments, [3].

Particle images of 3D fluid flows were captured with a camera PIVCAM 13.8 (TSI Shoreview, MN, US) synchronized with two pulsed lasers (MiniLase II-30 (New Wave research, Fremont, CA, US), both mounted on a straight microscope Eclipse TE600 (Nikon, Melville, NY, US). Images of particles $1\mu m$ in diameter were taken on an (x,y) plane at different heights z above the electrodes, their in-plane velocity is extracted using a custom μPIV software [29]. The algorithm described above was then used to extract the out of plane velocity component. The images were taken using an infinity corrected lenses (Nikon $M=20$, $NA=0.50$). To obtain a larger field of view and see the entire vortices, we use a relay lens with magnification $0.5\times$ thereby reducing the optical system magnification down to $M=10$.

The AC electrothermal fluid flow experiments, Figure 1.1, are performed in a $6mm$ diameter and $315\mu m$ deep circular PDMS chamber, bonded between a $1.1mm$ thick PCB board (FR4) and a $150\mu m$ thick glass cover slip with double sided tape (444 3M, St Paul, MN, US). The micro-chamber is filled with PBS solution diluted 10 times down to a conductivity of $\sigma = 1.84mS.cm^{-1}$. The room temperature is set to $T_r = 23°C$. An AC electric field is generated between three copper electrodes plated with $25-75$nm of gold. The electrodes are separated by a $200\mu m$ gap, on which a 20μ thick black soldermask was deposited to limit FR4 background fluorescence. A high frequency sinusoidal signal of $1MHz$ with peak to peak voltage $V = 17.5V_{pp}$ is applied to both side $500\mu m$ wide electrodes, the opposite phase signal is applied to the central $200\mu m$ wide electrode. High frequency signal is chosen to limit electrolysis and AC electro-osmosis, which occur at low frequency [30].

3.2 Numerical Model

A 2D finite element model is computed using COMSOL Multiphysics v4.3 software COMSOL Inc., Stockholm, Se). As explained in our previous paper [3], this 2D model includes the PCB board the, PDMS room, the electrodes and the 10 times diluted PBS buffer. The electrical potential and the temperature distribution are computed in half of the symmetric microfluidic room, solving sequentially electric fields, thermal conduction and Navier Stokes equations with an relative error of 10^{-3}. For a better accuracy with experimental data, the reference velocities (u_r,w_r) are computed using our enhanced model which takes into account viscosity and electrical conductivity temperature dependence.

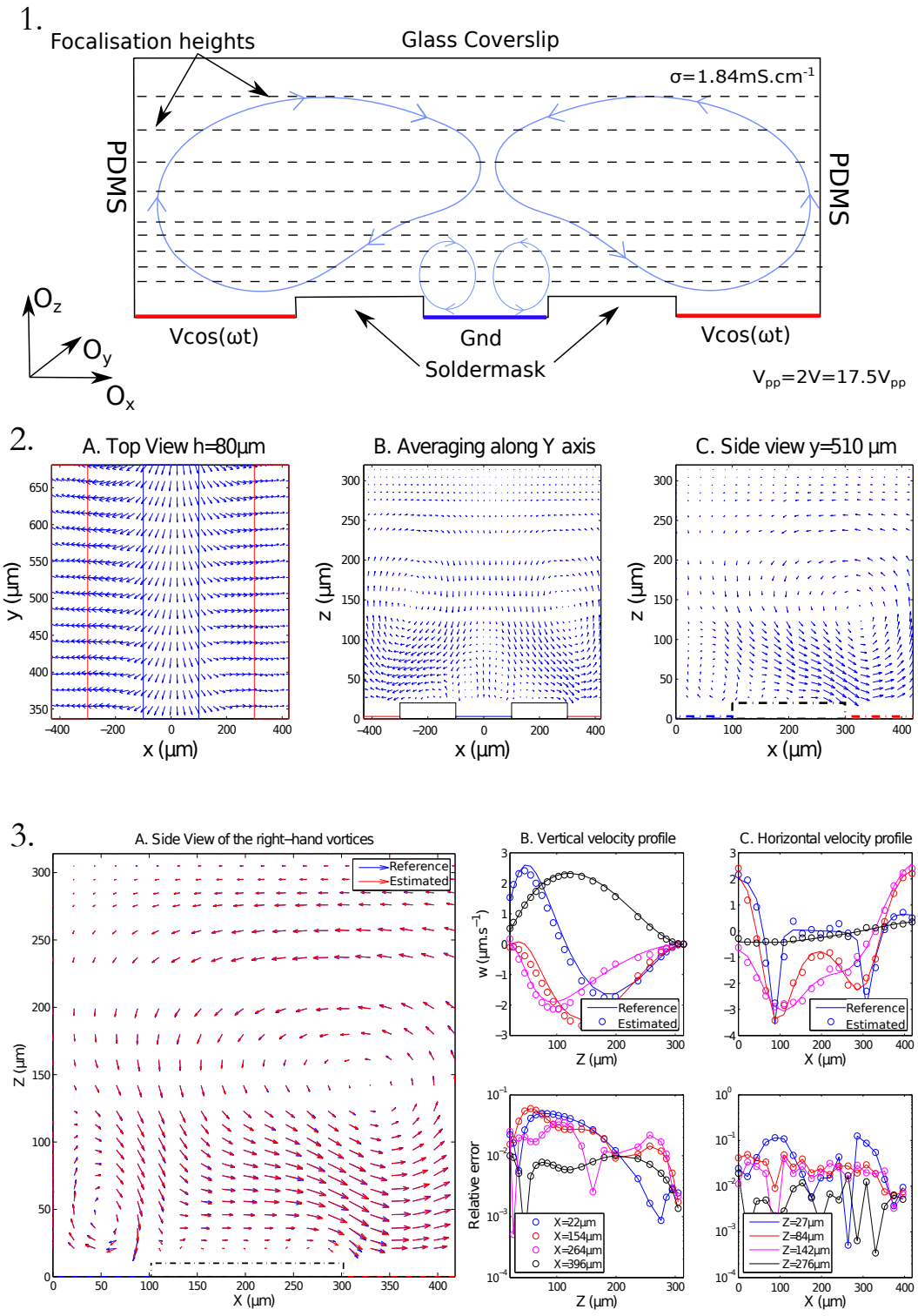

Figure 1: 1. Sideview of the experimental device. Electrothermal vortices are generated with 3 electrodes (blue: ground, red: phase $^1/_2 V_{pp}\cos(2\pi ft)$, with $f = 1$Mhz, and $V_{pp} = 2V = 17.5V_{pp}$). 2. Experimental μPIV velocity field. 2.A. Top view of the the in-plane velocity field (u_{ex},v_{ex}) acquired experimentally. 2.B. Side view of the velocity field (u_{ex},w_{ex}) after averaging along the electrode (*i.e.* Y axis). 2.C. Side view of the right side of the vortices (u_{ex},w_{ex}) 3. Comparison between reference out-of-plane component (w_r) (computed with COMSOL) and the out-of-plane velocity component w_e estimated from from the in-plane velocity component u (computed with COMSOL), to which Brownian motion and μPIV depth of correlation errors are added. 3.A. Side-view of the right side of the vortices. 3.B. Vertical and Horizontal velocity profiles and quadratic nomalized error.

4. Results and Discussion

The out of plane velocity component is computed using the method described above (Fig. 1 2.B and 2.C) using in-plane velocity fields acquired by μPIV. (Fig. 1 2.A). Given the high flow gradients near the electrodes, the spacing between each vertical position is small ($6\mu m$), whereas the spacing can reach $40\mu m$ in the upper part of the chamber. The electrodes, on which ground and phase are applied are displayed in blue and red, respectively. Because of the shape factor of the electrodes, the ETH flow is mainly 2D in Oxz plane. There is a flow along the electrode (Oy), which can be explained by the recirculation of vortices in the circular micro-chamber which has very small gradient ($\frac{dv}{dy} \approx 0$). Therefore the recirculation doesn't induce significant change on the vertical component. The flow can be thus averaged along the y axis $n_y = 17$ times, decreasing the uncertainty by a factor $\sqrt{n_y}$ as shown in Figure 1.2.B. A slight asymmetry is noticed which is certainly due to the electrode geometry inaccuracy induced during the PCB fabrication process. Figure 1.2.C shows a vertical slice of the right-hand side vortices without averaging.

Using a 2D COMSOL model previously developed [3], side views of ACET flows (u,w) are plotted in Figure 1.3.A. The vortex configuration closely matches our 2D numerical model. The 2D COMSOL velocity field is consistent with the experimental values, showing the reliability of our model. Vertical and horizontal profiles of the out-of-plane velocity and the relative computational error are plotted in Figure 1.3.B & C. The relative errors shown in 1.3.B and C are computed as the difference between the reference out-of-plane velocity components called w_r (computed with 2D COMSOL model) and the estimated out-of-plane velocity components w_e (computed from COMSOL in-plane velocity component, taking into account a measured unbias random error $\varepsilon_{xy} = 1.2\%$ and an estimated depth of correlation error $\delta_z = 11.6\mu m$). The normalized error is estimated to be on average $\varepsilon_z = 3.5\%$.

5. Conclusion

We have developed a 3D μ PIV method which is highly accurate using a standard epifluorescent microscope and demonstrated its use on a 3-D AC electrothemal fluid flow. The technique is a natural extension of 2-D μPIV, and does not require additional equipment. The error for in-plane velocity is approximately 1.2% while the out of plane error is approximately 3.5% full scale.

REFERENCES

[1] JG Santiago, ST Wereley, CD Meinhart, DJ Beebe, and RJ Adrian. A particle image velocimetry system for microfluidics. *Experiments in Fluids*, 1998.

[2] Steven T Wereley and Carl D Meinhart. Recent Advances in Micro-Particle Image Velocimetry. *Annu. Rev. Fluid Mech.*, 2010.

[3] Sophie Loire, Paul Kauffmann, Igor Mezić, and Carl Meinhart. A Theoretical and Experimental Study of Electrothermal Flows . *Journal Of Physics, Applied Physics D*, 2012.

[4] Ralph Lindken, Massimiliano Rossi, Sebastian Gro German sz ligature e, and Jerry Westerweel. Micro-Particle Image Velocimetry (PIV): Recent developments, applications, and guidelines. *Lab on a Chip*, 2009.

[5] Dazhi Wang, Marin Sigurdson, and Carl D Meinhart. Experimental analysis of particle and fluid motion in ac electrokinetics. *Experiments in Fluids*, 2005.

[6] Mitsuhisa Ichiyanagi, Seiichi Sasaki, Yohei Sato, and Koichi Hishida. Micro-PIV/LIF measurements on electrokinetically-driven flow in surface modified microchannels. *Journal of Micromechanics and Microengineering*, 2009.

[7] F Bottausci, Igor Mezić, CD Meinhart, and C Cardonne. Mixing in the shear superposition micromixer: three-dimensional analysis. *Philosophical Transactions of the Royal Society A: Mathematical, Physical and Engineering Sciences*, 2004.

[8] Axel Günther, Manish Jhunjhunwala, Martina Thalmann, Martin A Schmidt, and Klavs. F. Jensen. Micromixing of Miscible Liquids in Segmented GasLiquid Flow. *Langmuir*, 2005.

[9] H Kinoshita, S Kaneda, T Fujii, and M Oshima. Three-dimensional measurement and visualization of internal flow of a moving droplet using confocal micro-PIV. *Lab on a Chip*, 2006.

[10] Y Sugii, S Nishio, and K Okamoto. In vivo PIV measurement of red blood cell velocity field in microvessels considering mesentery motion. *Physiological measurement*, 2002.

[11] Peter Vennemann, Kenneth T Kiger, Ralph Lindken, Bianca C W Groenendijk, Sandra Stekelenburg-de Vos, Timo L M ten Hagen, Nicolette T C Ursem, Rob E Poelmann, Jerry Westerweel, and Beerend P Hierck. In vivo micro particle image velocimetry measurements of blood-plasma in the embryonic avian heart. *Journal of Biomechanics*, 2006.

[12] Y Fu, R Kunz, and J. Wu. Study of Local Hydrodynamic Environment in Cell-Substrate Adhesion Using Side-View PIV Technology. *PloS one*, 2012.

[13] Renaud Poincloux, Olivier Collin, Floria Lizárraga, Maryse Romao, Marcel Debray, Matthieu Piel, and Philippe Chavrier. Contractility of the cell rear drives invasion of breast tumor cells in 3D Matrigel. *Proceedings of the National Academy of Sciences*, 2011.

[14] CT Yang and HS Chuang. Measurement of a microchamber flow by using a hybrid multiplexing holographic velocimetry. In *Experiments in Fluids*, 2005.

[15] Shin-ichi Satake, Tomoaki Kunugi, Kazuho Sato, Tomoyoshi Ito, and Jun Taniguchi. Three-Dimensional Flow Tracking in a Micro Channel with High Time Resolution Using Micro Digital-Holographic Particle-Tracking Velocimetry. *Optical Review*, 2005.

[16] Shin-ichi Satake, Tomoaki Kunugi, Kazuho Sato, Tomoyoshi Ito, Hiroyuki Kanamori, and Jun Taniguchi. Measurements of 3D flow in a micro-pipe via micro digital holographic particle tracking velocimetry. *Measurement Science and Technology*, 2006.

[17] Ralph Lindken, Jerry Westerweel, and Bernhard Wieneke. Stereoscopic micro particle image velocimetry. *Experiments in Fluids*, 2006.

[18] Sang Youl Yoon and Kyung Chun Kim. 3D particle position and 3D velocity field measurement in a microvolume via the defocusing concept. *Measurement Science and Technology*, 2006.

[19] JS Park, CK Choi, and KD Kihm. Optically sliced micro-PIV using confocal laser scanning microscopy (CLSM). *Experiments in Fluids*, 2004.

[20] M.S. Pommer. Fluid mechanic manipulations on cells. 2007.

[21] A Chatterjee. An introduction to the proper orthogonal decomposition. *Current Science*, 2000.

[22] Azriel Rosenfeld and Avinash C Kak. *Digital Picture Processing*. Academic Press, Inc., 1982.

[23] C A Andrews and J M Davies. IEEE Xplore - Adaptive data compression. In *Proceedings of the IEEE*, 1967.

[24] L Sirovich. Chaotic dynamics of coherent structures. *Physica D: Nonlinear Phenomena*, 1989.

[25] Rudolph W Preisendorfer and Curtis D Mobley. *Principal component analysis in meteorology and oceanography*. Elsevier Science Ltd, 1988.

[26] Josh Danczyk and Krishnan Suresh. Algebraic Dimensional Reduction for Microfluidic Simulation. *Journal of Computing and Information Science in Engineering*, 2009.

[27] Philippe Druault and Christophe Chaillou. Use of Proper Orthogonal Decomposition for reconstructing the 3D in-cylinder mean-flow field from PIV data. *Cr Mecanique*, 2007.

[28] Abraham Savitzky and M J E Golay. Smoothing and Differentiation of Data by Simplified Least Squares Procedures. *Analytical Chemistry*, 1964.

[29] Carl D Meinhart, Steve T. Wereley, and Juan G. Santiago. PIV measurements of a microchannel flow. *Experiments in Fluids*, 1999.

[30] A. Castellanos, A. Ramos, A. González, N. G. Green, and H. Morgan. Electrohydrodynamics and dielectrophoresis in microsystems: scaling laws. *Journal of Physics D: Applied Physics*, 2003.